

Geophysical Research Letters®



RESEARCH LETTER

10.1029/2024GL114142

Key Points:

- Background wind speeds and urban heat islands (UHIs) are correlated and seem to exert opposing influences on downwind precipitation enhancement
- Background wind speeds can better explain the spatiotemporal variations of downwind precipitation enhancement than UHIs
- An increase in background wind speed, coupled with urban-rural momentum roughness length difference, leads to stronger air convergence

Supporting Information:

Supporting Information may be found in the online version of this article.

Correspondence to:

X.-T. Zheng,
zhengxt@ouc.edu.cn

Citation:

Ding, M., Zheng, X.-T., Li, D., & Sun, T. (2025). Background wind speeds outweigh urban heat islands in downwind precipitation enhancement by cities. *Geophysical Research Letters*, 52, e2024GL114142. <https://doi.org/10.1029/2024GL114142>

Received 8 DEC 2024
Accepted 30 MAY 2025

Author Contributions:

Conceptualization: Xiao-Tong Zheng, Dan Li, Ting Sun
Data curation: Mingze Ding
Formal analysis: Mingze Ding
Funding acquisition: Xiao-Tong Zheng
Investigation: Mingze Ding, Dan Li
Methodology: Xiao-Tong Zheng, Dan Li, Ting Sun
Resources: Dan Li
Supervision: Xiao-Tong Zheng, Ting Sun
Validation: Dan Li, Ting Sun
Visualization: Dan Li
Writing – original draft: Mingze Ding, Xiao-Tong Zheng, Dan Li, Ting Sun
Writing – review & editing: Xiao-Tong Zheng, Dan Li, Ting Sun

© 2025. The Author(s).

This is an open access article under the terms of the [Creative Commons Attribution License](https://creativecommons.org/licenses/by/4.0/), which permits use, distribution and reproduction in any medium, provided the original work is properly cited.

Background Wind Speeds Outweigh Urban Heat Islands in Downwind Precipitation Enhancement by Cities

Mingze Ding¹ , Xiao-Tong Zheng¹ , Dan Li^{2,3} , and Ting Sun⁴

¹State Key Laboratory of Physical Oceanography, Ocean University of China, Qingdao, China, ²Department of Earth and Environment, Boston University, Boston, MA, USA, ³Department of Mechanical Engineering, Boston University, Boston, MA, USA, ⁴Department of Risk and Disaster Reduction, University College London, London, UK

Abstract Ample evidence shows that cities can enhance precipitation in the downwind region due to the urban heat island (UHI) effect and the high momentum roughness of urban land. Surprisingly, global observational results show that the downwind enhancement of precipitation caused by large metropolitan areas is weaker under conditions of stronger surface UHIs. This is because stronger UHIs tend to be associated with lower background wind speeds, while the downwind enhancement of precipitation is stronger with higher background wind speeds. These results suggest a competition between thermodynamic and dynamic factors in regulating the downwind enhancement of precipitation, with the background wind speed playing a more important role than the UHI effect. By considering the urban-rural difference in momentum roughness length, a simple model is utilized to qualitatively explain the link between the downwind enhancement of precipitation and background wind speed.

Plain Language Summary Traditionally, more heat (i.e., thermodynamic factor) and increased roughness (i.e., dynamic factor) in cities can lead to greater upward movement of air, which promotes precipitation, particularly in the downwind areas of cities. Although both mechanisms have been studied, their interactions under varying background wind speeds have not yet been explored. Our global results show that the downwind enhancement of precipitation caused by large metropolitan areas is weaker with stronger urban heat island effects but stronger with higher background wind speeds, suggesting a competition between thermodynamic and dynamic factors and background wind speeds outweighing urban heat islands in enhancing precipitation downwind of cities. This work provides new insights into the link between urban surface characteristics and regional hydroclimates.

1. Introduction

Over the past 200 years, the global population has increased sevenfold and the urban population has increased from 3% to over 50% (Nations, 2018). Urban development so fundamentally transforms the preexisting biophysical landscape that a city creates its own climate (Y. Li et al., 2024). Understanding changes in climate and atmospheric composition caused by urbanization is crucial for providing the scientific data needed to design, manage, and operate safer, healthier, more sustainable, and resilient cities (Oke et al., 2017).

Since the Laporte precipitation anomaly—unusually high precipitation levels downwind of Chicago—was reported (Changnon, 1968), it was conjectured that this anomaly may be linked to urban effects (Changnon et al., 1976). Detailed studies from the Metropolitan Meteorological Experiment (METROMEX) confirmed that cities can influence precipitation patterns (Braham & Dungey, 1978; Changnon et al., 1971, 1991), particularly in the downwind areas of cities (Changnon, 2016). Since then, the downwind enhancement of precipitation by cities has been widely reported for cities over the United States (Lu et al., 2024; Niyogi et al., 2017), Europe (Lorenz et al., 2019), East Asia (L. Yang et al., 2014), and South Asia (Sarangi et al., 2018). This downwind precipitation enhancement by cities is now recognized as a global signal (Sui et al., 2024), increasing rainfall-related hazards (L. Yang et al., 2024).

Cities tend to be warmer than surrounding rural areas, a phenomenon now labeled as the urban heat island (UHI) effect (D. Li et al., 2024; Manoli et al., 2019; Oke et al., 2017). Multiple studies have shown a relation between the UHI effect and precipitation enhancement (Huang et al., 2022; Jiang et al., 2023; Zhu et al., 2017). Urban sensible heat and anthropogenic heat fluxes act as the energy source to enhance upward vertical motions and atmospheric instability (W. Yang et al., 2017), which are conducive to cloud formation and rainfall (Marelle et al., 2020).

Moreover, the high momentum roughness length of urban land leads to weaker near-surface horizontal wind over cities, which further results in airflow convergence and upward motions that could affect precipitation patterns (Ao et al., 2022; Chen et al., 2017).

However, the downwind enhancement of precipitation is not solely determined by urban characteristics, but also affected by other environmental factors such as the background wind speed. In the studies of mid-latitude cities, it is found that the precipitation enhancement caused by cities can move far downwind under the influences of background wind (Marelle et al., 2020; Zhang et al., 2015). In contrast, studies also have found that under conditions of weak climatological background winds over a tropical city, downwind enhancement was not observed (Y. Li et al., 2020). Instead, the precipitation enhancement occurred over the city. These studies suggest that the background wind speed plays an important role in determining the location of precipitation maxima. By analyzing 27 selected cities across the USA, Lu et al. (2024) found that the location of precipitation maxima moves downwind with higher background wind speeds.

Collectively, both urban characteristics (such as the UHI effect) and environmental conditions (such as the background wind speed) play important roles in affecting the downwind precipitation enhancement (Hu et al., 2023; Pimonsree et al., 2022; L. Yang et al., 2024). However, these two factors are strongly correlated. For example, the UHI effect tends to weaken under stronger winds (Arnfield, 2003). The interplay of UHI and background wind speed in the context of downwind precipitation enhancement has not been disentangled, which motivates our work.

2. Data and Methodology

2.1. Data

We use the Integrated Multi-satellite Retrievals for Global Precipitation (IMERG_Final) data, a Level 3 multi-satellite product from the Global Precipitation Measurement mission, with a spatial resolution of 0.1° and a monthly temporal resolution from 2001 to 2020.

We also use 850 hPa winds with a spatial resolution of 0.25° and a monthly temporal resolution from 2001 to 2020 from the European Centre for Medium-Range Weather Forecasts Reanalysis v5 (ERA5) product. The 850 hPa winds better indicate weather system movements than higher-level winds (Y.-Y. Liu et al., 2021), and being near the atmospheric boundary layer top (for near-sea-level locations), they represent background wind speed unaffected by surface conditions. All wind data is resampled from 0.25° to 0.1° spatial resolution using the bilinear interpolation. Since the wind fields exhibit good spatial continuity and we do not require highly precise wind direction data, the errors introduced by resampling are acceptable.

For urban identification, we employ the Terra and Aqua combined Moderate Resolution Imaging Spectroradiometer (MODIS) Land Cover Type Level 3 (MCD12C1) data with a spatial resolution of 0.05° and annual temporal resolution from 2001 to 2020. MODIS data is resampled to 0.1° spatial resolution to match our precipitation data using the bilinear interpolation. A pixel is defined as an urban pixel if the proportion of urban surface exceeds 50%. The annual variation of land cover types is not considered in this analysis.

To quantify the surface UHI intensity, we use the monthly scale and city scale satellite-derived surface UHI data from Chakraborty and Lee (2019), calculated as the difference between urban and rural surface temperatures based on MODIS land surface temperature data and validated against multi-city studies. The surface UHI value is directly provided by this product and the details about the data product can be found in Chakraborty and Lee (2019). We compute the daily UHI intensity by averaging the daytime and nighttime UHI values. Given the uncertainties in satellite observations during wet days, we also calculate the surface UHI intensity from skin temperature data provided by the Global Land Data Assimilation System (GLDAS) (2001–2020, 0.25° spatial and monthly temporal resolution) (Harmay et al., 2021). The skin temperature data from GLDAS is resampled to 0.1° spatial resolution using the bilinear interpolation. Considering the error introduced by interpolation, the satellite and GLDAS data are used for mutual verification.

2.2. Methodology

To analyze downwind precipitation enhancement by cities, we extract all trans-urban wind paths worldwide at a monthly scale from 2001 to 2020 (Figure S1 in Supporting Information S1). To do so, we first identify each pixel's

neighboring (upwind and downwind) pixels using its 850 hPa wind direction, which is calculated as $\arctan(V/U)$ with V being the meridional wind and U being the zonal wind. Then we start a search process from each urban pixel, looking for its downwind pixel. We will continue this search in the downwind direction until three consecutive pixels are no longer urban pixels. These three consecutive non-urban pixels are considered as the downwind part of this wind path. Similarly, we will search in the upwind direction and three consecutive non-urban pixels are considered as the upwind part of this wind path. All urban pixels along this wind path are considered as the urban part of this wind path, with the non-urban pixels in between them removed. In this way, the upwind and downwind parts are always of length 0.3° , but the urban part can be shorter or longer than 0.3° . The length of the urban part is called the urban width. Because the urban part is defined based on the wind path, it may vary from month to month. The urban part defined this way is not necessarily a specific city, which is defined as a group of adjacent urban pixels in our study. In some cases, the urban part of a wind path can include multiple cities.

This process results in 1,386,073 trans-urban wind paths from 2001 to 2020, which are then used to explore the relation between downwind enhancement of precipitation and urban width. The main analysis focuses on 1,459 wind paths with the urban width larger than 1.2° . The urban part of these wind paths with large urban widths may be a single large city or a group of small but neighboring cities. For simplicity, the urban part of these wind paths with large urban widths will be called a large metropolitan area.

The wind paths with large urban widths are scattered globally. The low-latitude region ($<30^\circ\text{N/S}$) includes 153 wind paths, and the mid-to-high-latitude region ($>30^\circ\text{N/S}$) includes 1,306 wind paths. We also explore seasonal variations of such wind paths for the mid-to-high-latitude region in the Northern Hemisphere ($>30^\circ\text{N}$), where DJF (December-January-February) includes 339 wind paths, MAM (March-April-May) includes 318 wind paths, JJA (June-July-August) includes 312 wind paths, and SON (September-October-November) includes 337 wind paths.

We quantify the surface UHI intensity and background wind speed of the trans-urban wind paths with urban widths larger than 1.2° . Using the satellite-derived surface UHI intensity data, the surface UHI intensity of each trans-urban wind path is calculated by averaging the UHI intensities of all urban pixels along the wind path. Using the GLDAS data, the surface UHI intensity of each trans-urban wind path is calculated by the difference in the average skin temperature between the urban pixels and rural pixels along the wind path. The background wind speed of each trans-urban wind path is calculated as the average ERA5 850 hPa wind speed of all pixels along the path.

Based on the surface UHI intensities and background wind speeds, we further group trans-urban wind paths into different groups. Based on the first tertile (0.61 K) and second tertile (1.08 K) of UHI intensities of all studied trans-urban wind paths, we classify wind paths into three groups: wind paths with Low-UHI (<0.61 K), wind paths with Mid-UHI (0.61–1.08 K), and wind paths with High-UHI (>1.08 K). Similarly, based on the first tertile (4.45 m/s) and second tertile (7.82 m/s) of ERA5 850 hPa wind speed data, we classify wind paths into three groups: wind paths with Low-wind (<4.45 m/s), wind paths with Mid-wind (4.45–7.82 m/s), and wind paths with High-wind (>7.82 m/s).

Since wind path lengths vary globally, we standardize the urban part of each wind path to a uniform width (0.3°) to enable comparison of precipitation along different wind paths. The precipitation along the urban part is rescaled using linear interpolation. Considering that precipitation varies strongly with cities, each precipitation profile is rescaled to a range of [0, 1] using min-max normalization. Both actual and normalized precipitation are considered in our study.

The bootstrap method, which has been widely used for analyzing climatic data (Espinosa & Portela, 2022; Xu et al., 2015), is used to quantify the uncertainty in our data (Stine, 1989). The basic idea of the bootstrap method is that inference about a population from sample data can be modeled by resampling the sample data and performing inference about a sample from resampled data. Our study uses a default resampling frequency of 10,000 iterations.

3. Results

3.1. Downwind Enhancement of Precipitation Caused by Large Metropolitan Areas

We start our analysis by exploring the relationship between the downwind precipitation enhancement and urban width. This is motivated by previous observational studies suggesting that the urban impact on precipitation is

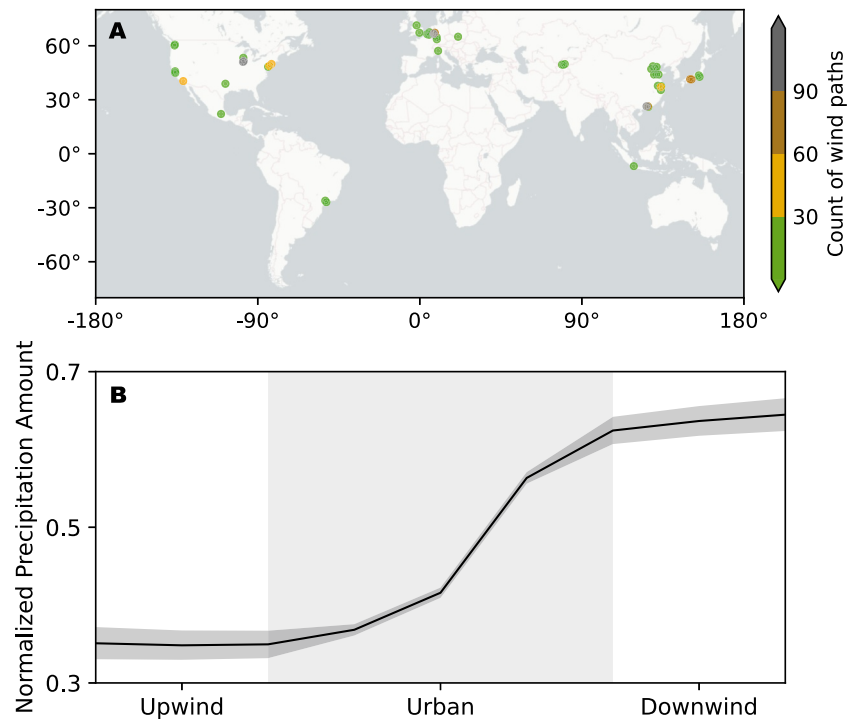


Figure 1. Downwind precipitation enhancement by large metropolitan areas. (a) Location of studied cities (51 in total, with 9 in low-latitude region and 42 in mid-to-high-latitude region). The color represents the number of wind paths for each city from 2001 to 2020. Note that cities close to each other might be on a single wind path. (b) The global average monthly precipitation along the trans-urban wind paths. To account for global variations in precipitation, each profile is rescaled to a range of [0, 1] using min-max normalization. The fill areas refer to the 95% confidence intervals calculated by the bootstrap method.

more noticeable in larger cities (Wai et al., 2017; L. Yang et al., 2024). Moreover, idealized or semi-idealized simulation studies also showed that precipitation modification increases with city size (Schmid & Niyogi, 2013; Zhu et al., 2017). Our results indicate that downwind precipitation enhancement does not occur for all tran-urban wind paths, but only for wind paths with large urban widths, particularly those with urban widths greater than 1.2° (Figure S2 in Supporting Information S1). Therefore, we restrict our subsequent analysis to wind paths with urban widths greater than 1.2° (Figure 1a).

When averaged over all the selected wind paths, a consistent downwind precipitation enhancement emerges, as shown in both the normalized precipitation amount (Figure 1b) and the actual precipitation amount (Figure S3 in Supporting Information S1). This is broadly consistent with previous studies (see a recent meta-analysis by J. Liu and Niyogi (2019), L. Yang et al. (2024), and Lu et al. (2024)) and the traditional framework arising from the METROMEX campaign (Braham & Dungey, 1978; Changnon et al., 1976, 1991).

3.2. Relation Between Downwind Precipitation Enhancement and Surface UHI and Background Wind Speed

Building upon the observed downwind precipitation enhancement and the widely acknowledged important role of the UHI effect, we explore whether such an enhancement is stronger with stronger surface UHIs. Here, we classify all studied wind paths into three categories based on satellite-derived surface UHI intensity compiled by Chakraborty and Lee (2019) and compare the downwind precipitation enhancement across these three categories (Figure 2a). Surprisingly, we find that the downwind precipitation enhancement is weaker along wind paths with higher surface UHI intensities. Considering the high uncertainties in the satellite observation of surface UHI intensity on wet days, we also use GLDAS-modeled skin temperature to quantify the surface UHI intensity. We still observe this negative relation between the surface UHI intensity and downwind precipitation enhancement (Figure S4 in Supporting Information S1). Moreover, stronger downwind enhancement is observed along wind paths with negative UHIs than in wind paths with positive UHI (Figure S5 in Supporting Information S1).

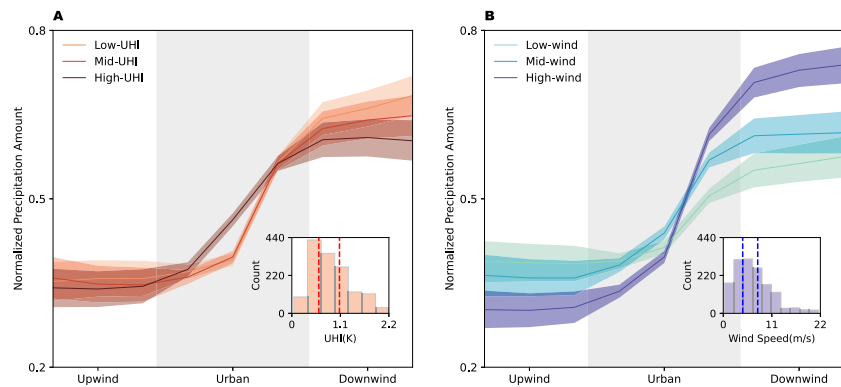


Figure 2. The relation between downwind precipitation enhancement and surface urban heat island (UHI) and background wind speed. (a) Downwind enhancement of precipitation across different surface UHI intensities. (b) Downwind enhancement of precipitation across different background wind speeds at 850 hPa. The filled areas refer to the 95% confidence intervals calculated by the bootstrap method. The insets show the histogram of surface UHI intensities and background wind speeds associated with the studied wind paths, with dashed lines indicating the first and second tertiles, respectively.

By analyzing 27 cities across the continental United States, Lu et al. (2024) found that the location of precipitation maxima shifted downwind as the background wind speed increased. Motivated by their work, we also explore the magnitude of downwind precipitation enhancement at different background wind speeds. For this analysis, we classify all studied wind paths into three categories based on the 850 hPa wind speed and compare the downwind enhancement patterns across these categories (Figure 2b). Here, we find a positive relation between downwind precipitation enhancement and background wind speed, with stronger downwind enhancement under conditions of higher background wind speeds. This finding differs from, but complements, the study by Lu et al. (2024), which examined the location of downwind precipitation enhancement but did not explore the magnitude of downwind precipitation enhancement.

The important role of background wind speed as shown in Figure 2b also helps explain the seemingly counter-intuitive relation between the surface UHI intensity and downwind precipitation enhancement (Figure 2a and Figure S4 in Supporting Information S1), as the surface UHI intensity tends to be negatively correlated with the background wind speed (Arnfield, 2003). This negative correlation is also demonstrated in our analysis (Figure S6 in Supporting Information S1). This negative correlation is physically intuitive, as stronger wind speeds can effectively advect heat away from its source, preventing local heat accumulation and promoting cooling in the urban environment (Hsieh & Huang, 2016). Additionally, higher background wind leads to more mixing and thus weaker urban-rural temperature differences (or weaker UHI intensities) (Lundquist & Mirocha, 2008).

In summary, our results suggest a competition between the background wind speed and surface UHI intensity in enhancing downwind precipitation, with the former playing a more important role than the latter. Next, we will provide further evidence to corroborate this argument.

3.3. Spatiotemporal Variations of Downwind Precipitation Enhancement and Their Relation to Background Wind Speed

By dividing the studied wind paths into low-latitude ($<30^{\circ}\text{N/S}$) and mid-to-high-latitude ($>30^{\circ}\text{N/S}$), we discover significant differences in both background wind speeds and downwind enhancement patterns between the two groups (Figure 3a). In mid-to-high-latitude wind paths, precipitation increases primarily in the downwind region due to high background wind speeds, whereas in low-latitude wind paths with low background wind speeds, precipitation increases primarily within the urban area (Figure 3a). This is consistent with a previous case study in Kuala Lumpur, where strong intensification of rainfall extremes occurred over the city itself instead of the downwind region (Y. Li et al., 2020). The low climatological wind speeds were suggested as the cause of the absence of downwind precipitation enhancement (Y. Li et al., 2020).

Focusing on the downwind precipitation enhancement in wind paths located north of 30°N , we also find higher background wind speed and stronger downwind precipitation enhancement in the winter season (DJF), but lower

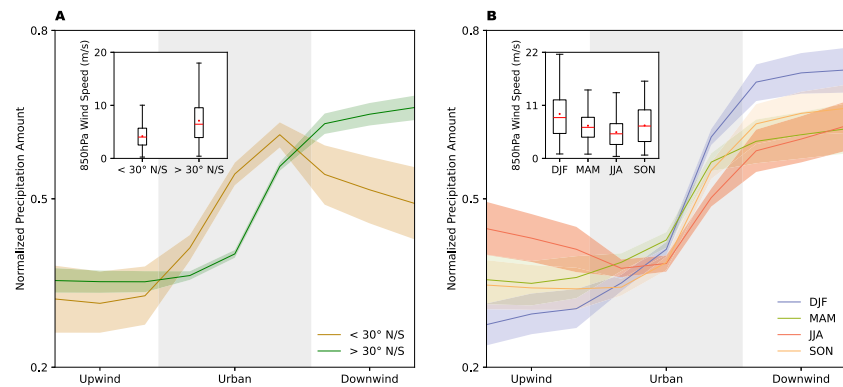


Figure 3. Spatiotemporal variations of downwind precipitation enhancement and their relations to background wind speed. (a) Downwind precipitation enhancement in low-latitude region ($<30^{\circ}\text{N/S}$) and mid-to-high-latitude region ($>30^{\circ}\text{N/S}$). (b) Downwind precipitation enhancement across different seasons for wind paths above 30°N . The fill areas refer to the 95% confidence intervals calculated by the bootstrap method. The insets show a box plot of background wind speed along the studied wind paths. In the box plots, the 25th and 75th percentiles are shown as the lower and upper edges of the boxes while the median is marked by the center red line, and the average is marked as the red circle. The upper and lower whiskers show the 97.5th and the 2.5th percentiles, respectively.

background wind speeds and weaker downwind precipitation enhancement in the summer season (JJA) (Figure 3b). The difference in downwind precipitation enhancement between summer season and winter season is also shown in the actual precipitation amount (Figure S7 in Supporting Information S1). In other words, the seasonal variations of background wind speed are also consistent with those of downwind precipitation enhancement.

Overall, these results show that the spatiotemporal variations of downwind precipitation enhancement are similar to those of background wind speeds. In contrast, the spatiotemporal variations of surface UHI intensities do not coincide with those of downwind precipitation enhancement (Figure S8 in Supporting Information S1). The analysis above suggests that background wind speed is a key variable when explaining the enhancement of downwind precipitation by cities.

3.4. Background Wind Speed Increases Airflow Convergence

In this section, we propose an explanation for the relation between a higher background wind speed and a stronger downwind enhancement of precipitation. Here, we use an idealized two-layer model to analyze the urban response under different background wind speeds (see Text S1 in Supporting Information S1). Two assumptions are applied in the idealized two-layer model, which are widely used in previous studies (Barlow, 2014; Karlsson, 1986; B. Liu et al., 2024; Wieringa, 1986): First, the wind speed at the upper layer is exclusively determined by weather conditions, and as a result, it is identical in urban and rural areas (i.e., represented by the background wind speed). Second, the wind speed at the lower layer (i.e., within the atmospheric boundary layer) fits the logarithmic wind profile according to the Monin-Obukhov similarity theory and thus is reduced more over cities with higher momentum roughness length than in rural areas.

Based on these two assumptions, we can quantify the horizontal inflow of air under the lower layer (i.e., the height of L in Figure 4a) and further calculate the convergence under varying background wind speeds (Figure 4a). Our analytical approximation shows that the convergence in the lower layer is a linear function of the background wind speed (the blue dashed line in Figure 4b) for the specified urban and rural roughness lengths. The explanation for this relationship is that a stronger background wind speed, coupled with a higher momentum roughness length of urban land than that of rural land, leads to stronger airflow convergence across the urban-rural interface. The increased convergence potentially contributes to the enhanced precipitation (Knox et al., 2019), which will be transported downwind due to the horizontal background wind. Therefore, this analytical approximation qualitatively explains the positive relation between background wind speed and downwind precipitation enhancement (the black line in Figure 4b).

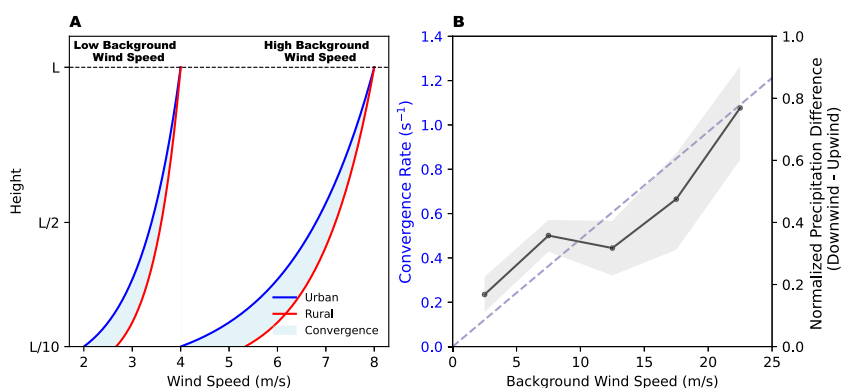


Figure 4. The convergence under different background wind speeds. (a) The urban and rural wind profiles under low and high background wind speed. (b) The calculated convergence and downwind precipitation enhancement across different background wind speeds. The horizontal convergence (the blue dashed line) is calculated using an idealized two-layer model (blue line) and integrated from $10/L$ to L where $L = 1,000$ m. The downwind precipitation enhancement is quantified as the normalized precipitation differences between downwind and upwind parts along the wind paths (black line). The filled areas refer to the 95% confidence intervals calculated by the bootstrap method.

The influences of winds on precipitation are complex. While here we focus on airflow convergence, such influences are likely also dependent on factors such as moisture content. More broadly, the interplay between UHIs, winds, and precipitation enhancement is complex, and our study further highlights the competition between thermodynamic and dynamic factors. It is worth noting that the urban signals explored in our study are based on global and monthly scale data, which hence might not necessarily reflect the mechanisms as reported in the previous specific case studies.

4. Discussion and Conclusion

In this study, we examine the downwind enhancement of precipitation by large metropolitan areas using satellite precipitation data and explore the relation between the downwind precipitation enhancement and two factors: surface UHI and background wind speed. Our results show that the downwind enhancement of precipitation is weaker with stronger UHI effects but stronger with higher background wind speeds. This suggests a competition between background wind speeds and surface UHIs in regulating the downwind precipitation enhancement, with the former playing a more important role than the latter. However, we acknowledge that assigning numerical values to quantify the relative contributions of these two factors remains a challenge.

For mid-latitude cities, most previous studies focus on the urban impact on summer precipitation. However, we find that the downwind precipitation enhancement is stronger in winter than in summer caused by the higher background wind speed (Figure 3b and Figure S7 in Supporting Information S1). Therefore, the urban impacts on winter precipitation should also be investigated. In low-latitude regions, we observe a distinct precipitation enhancement pattern compared to mid-to-high-latitude regions. This difference may arise from the combined influence of the UHI effect and background wind. Due to the stronger UHI effect (Figure S8 in Supporting Information S1) and weaker background wind speeds (Figure 3) in low-latitude regions, the increased precipitation does not move to the downwind areas as also demonstrated in a previous case study at Kuala Lumpur (Y. Li et al., 2020), which may increase the flood-related hazard risk in low-latitude cities.

The relationship between downwind enhancement and surface UHI and background wind is examined only for large metropolitan areas in our study, as capturing downwind enhancement signals in smaller cities proves challenging (Figure S2 in Supporting Information S1). It is worth noting that the influence of urban-induced aerosols on the spatial pattern of precipitation may lead to upwind-downwind precipitation differences (Fan et al., 2020; Sarangi et al., 2018); however, this factor is not discussed in our study. Additionally, our analysis is conducted at the monthly scale. Hence whether the results shown here would vary with different types of precipitation (Y. Li et al., 2021), such as convective and frontal precipitation, remains unknown and is left for future research.

Data Availability Statement

IMERG precipitation data set is available at Huffman et al. (2023). MODIS land use data set is available at Friedl and Sulla-Menashe (2015). ERA5 data is available at Hersbach et al. (2016). The GLDAS data set is available at Beaudoin and Rodell (2020). The satellite-based surface UHI data set is available at Chakraborty and Lee (2019). The code for extracting the trans-urban wind paths is available at (Ding, 2025).

Acknowledgments

This study was supported by the National Natural Science Foundation of China (42475026), Shandong Natural Science Foundation Project (ZR2019ZD12), and Taishan Scholars Project of Shandong Province (tsqn202306095). We thank two anonymous reviewers for their helpful comments on our manuscript.

References

- Ao, X., Yue, C., Yang, X., Deng, L., & Huang, W. (2022). Urbanization effects on rainfall processes induced by landfalling typhoon Lekima (2019) over the Shanghai metropolitan area. *Journal of Hydrometeorology*, 23(7), 1075–1093. <https://doi.org/10.1175/jhm-d-21-0170.1>
- Arnfield, A. J. (2003). Two decades of urban climate research: A review of turbulence, exchanges of energy and water, and the urban heat island. *International Journal of Climatology: a Journal of the Royal Meteorological Society*, 23(1), 1–26. <https://doi.org/10.1002/joc.859>
- Barlow, J. F. (2014). Progress in observing and modelling the urban boundary layer. *Urban Climate*, 10, 216–240. <https://doi.org/10.1016/j.uclim.2014.03.011>
- Beaudoin, H., & Rodell, M. (2020). GLDAS NOAA land surface model L4 monthly 0.25 x 0.25 degree v2. 1 [Dataset]. <https://doi.org/10.5067/SXAVCZFAQLNO>
- Braham, R. R., Jr., & Dungey, M. J. (1978). A study of urban effects on radar first echoes. *Journal of Applied Meteorology and Climatology*, 17(5), 644–654. [https://doi.org/10.1175/1520-0450\(1978\)017<0644:asoueo>2.0.co;2](https://doi.org/10.1175/1520-0450(1978)017<0644:asoueo>2.0.co;2)
- Chakraborty, T., & Lee, X. (2019). A simplified urban-extent algorithm to characterize surface urban heat islands on a global scale and examine vegetation control on their spatiotemporal variability. *International Journal of Applied Earth Observation and Geoinformation*, 74, 269–280. <https://doi.org/10.1016/j.jag.2018.09.015>
- Changnon, S. A. (1968). The La Porte weather anomaly—Fact or fiction? *Bulletin of the American Meteorological Society*, 49(1), 4–11. <https://doi.org/10.1175/1520-0477-49.1.4>
- Changnon, S. A. (2016). METROMEX: A review and summary.
- Changnon, S. A. Jr., Huff, F. A., & Semonin, R. G. (1971). METROMEX: An investigation of inadvertent weather modification. *Bulletin of the American Meteorological Society*, 52(10), 958–968. [https://doi.org/10.1175/1520-0477\(1971\)052<0958:maoiw>2.0.co;2](https://doi.org/10.1175/1520-0477(1971)052<0958:maoiw>2.0.co;2)
- Changnon, S. A. Jr., Semonin, R. G., & Huff, F. (1976). A hypothesis for urban rainfall anomalies. *Journal of Applied Meteorology and Climatology*, 15(6), 544–560. [https://doi.org/10.1175/1520-0450\(1976\)015<0544:ahfura>2.0.co;2](https://doi.org/10.1175/1520-0450(1976)015<0544:ahfura>2.0.co;2)
- Changnon, S. A., Shealy, R. T., & Scott, R. W. (1991). Precipitation changes in fall, winter, and spring caused by St. Louis. *Journal of Applied Meteorology and Climatology*, 30(1), 126–134. [https://doi.org/10.1175/1520-0450\(1991\)030<0126:pcifwa>2.0.co;2](https://doi.org/10.1175/1520-0450(1991)030<0126:pcifwa>2.0.co;2)
- Chen, Y.-C., Fröhlich, D., Matzarakis, A., & Lin, T.-P. (2017). Urban roughness estimation based on digital building models for urban wind and thermal condition estimation—Application of the Skyhelios model. *Atmosphere*, 8(12), 247. <https://doi.org/10.3390/atmos8120247>
- Ding, M. (2025). downwind_analysis: v1.0.0 [Software]. <https://doi.org/10.5281/zenodo.14868561>
- Espinosa, L. A., & Portela, M. M. (2022). Grid-point rainfall trends, teleconnection patterns, and regionalised droughts in Portugal (1919–2019). *Water*, 14(12), 1863. <https://doi.org/10.3390/w14121863>
- Fan, J., Zhang, Y., Li, Z., Hu, J., & Rosenfeld, D. (2020). Urbanization-induced land and aerosol impacts on sea-breeze circulation and convective precipitation. *Atmospheric Chemistry and Physics*, 20(22), 14163–14182. <https://doi.org/10.5194/acp-20-14163-2020>
- Friedl, M., & Sulla-Menashe, D. (2015). Mcd12c1 MODIS/TERRA+AQUA land cover type yearly L3 global 0.05deg CMG [Dataset]. NASA LP DAAC. <https://doi.org/10.5067/MODIS/MCD12C1.006>
- Harmay, N. S. M., Kim, D., & Choi, M. (2021). Urban heat island associated with land use/land cover and climate variations in Melbourne, Australia. *Sustainable Cities and Society*, 69, 102861. <https://doi.org/10.1016/j.scs.2021.102861>
- Hersbach, H., Bell, B., Berrisford, P., Biavati, G., Horányi, A., Muñoz Sabater, J., et al. (2016). ERA5 monthly averaged data on pressure levels from 1940 to present [Dataset]. <https://doi.org/10.24381/cds.6860a573>
- Hsieh, C.-M., & Huang, H.-C. (2016). Mitigating urban heat islands: A method to identify potential wind corridor for cooling and ventilation. *Computers, Environment and Urban Systems*, 57, 130–143. <https://doi.org/10.1016/j.compenvurbsys.2016.02.005>
- Hu, C., Tam, C.-Y., Loi, C. L., Cheung, K. K., Li, Y., Yang, Z.-L., et al. (2023). Urbanization impacts on tropical cyclone rainfall extremes—Inferences from observations and convection-permitting model experiments over South China. *Journal of Geophysical Research: Atmospheres*, 128(21), e2023JD038813. <https://doi.org/10.1029/2023jd038813>
- Huang, J., Fatichi, S., Mascaro, G., Manoli, G., & Peleg, N. (2022). Intensification of sub-daily rainfall extremes in a low-rise urban area. *Urban Climate*, 42, 101124. <https://doi.org/10.1016/j.uclim.2022.101124>
- Huffman, G., Stocker, E., Bolvin, D., Nelkin, E., & Tan, J. (2023). GPM IMERG final precipitation L3 1 month 0.1 degree x 0.1 degree v07 [Dataset]. <https://doi.org/10.5067/GPM/IMERG/3B-MONTH/07>
- Jiang, X., Zhang, D.-L., & Luo, Y. (2023). Influences of urbanization on an afternoon heavy rainfall event over the Yangtze river delta region. *Monthly Weather Review*, 151(3), 815–832. <https://doi.org/10.1175/mwr-d-22-0165.1>
- Karlsson, S. (1986). The applicability of wind profile formulas to an urban-rural interface site. *Boundary-Layer Meteorology*, 34(4), 333–355. <https://doi.org/10.1007/bf00120987>
- Knox, G., McInnes, C., Younger, P., & Sloan, W. (2019). Engineering artificial thermal mountains for large-scale water management and carbon drawdown. *Environmental Science: Water Research & Technology*, 5(2), 296–314. <https://doi.org/10.1039/c8ew00571k>
- Li, D., Wang, L., Liao, W., Sun, T., Katul, G., Bou-Zeid, E., & Maronga, B. (2024). Persistent urban heat. *Science Advances*, 10(15), ead7398. <https://doi.org/10.1126/sciadv.ad7398>
- Li, Y., Beeton, R. J., Zhao, X., Fan, Y., Yang, Q., Li, J., & Ding, L. (2024). Advancing urban sustainability transitions: A framework for understanding urban complexity and enhancing integrative transformations. *Humanities and Social Sciences Communications*, 11(1), 1–14. <https://doi.org/10.1057/s41599-024-03598-x>
- Li, Y., Fowler, H. J., Argüeso, D., Blenkinsop, S., Evans, J. P., Lenderink, G., et al. (2020). Strong intensification of hourly rainfall extremes by urbanization. *Geophysical Research Letters*, 47(14), e2020GL088758. <https://doi.org/10.1029/2020gl088758>
- Li, Y., Wang, W., Chang, M., & Wang, X. (2021). Impacts of urbanization on extreme precipitation in the Guangdong-Hong Kong-MACAU greater bay area. *Urban Climate*, 38, 100904. <https://doi.org/10.1016/j.uclim.2021.100904>
- Liu, B., Ma, X., Guo, J., Wen, R., Li, H., Jin, S., et al. (2024). Extending the wind profile beyond the surface layer by combining physical and machine learning approaches. *Atmospheric Chemistry and Physics*, 24(7), 4047–4063. <https://doi.org/10.5194/acp-24-4047-2024>

- Liu, J., & Niyogi, D. (2019). Meta-analysis of urbanization impact on rainfall modification. *Scientific Reports*, 9(1), 7301. <https://doi.org/10.1038/s41598-019-42494-2>
- Liu, Y.-Y., Li, L., Liu, Y.-S., Chan, P.-W., Zhang, W.-H., & Zhang, L. (2021). Estimation of precipitation induced by tropical cyclones based on machine-learning-enhanced analogue identification of numerical prediction. *Meteorological Applications*, 28(2), e1978. <https://doi.org/10.1002/met.1978>
- Lorenz, J. M., Kronenberg, R., Bernhofer, C., & Niyogi, D. (2019). Urban rainfall modification: Observational climatology over Berlin, Germany. *Journal of Geophysical Research: Atmospheres*, 124(2), 731–746. <https://doi.org/10.1029/2018jd028858>
- Lu, Y., Yu, Z., Albertson, J. D., Chen, H., Hu, L., Pendergrass, A., et al. (2024). Understanding the influence of urban form on the spatial pattern of precipitation. *Earth's Future*, 12(1), e2023EF003846. <https://doi.org/10.1029/2023ef003846>
- Lundquist, J. K., & Mirocha, J. D. (2008). Interaction of nocturnal low-level jets with urban geometries as seen in joint urban 2003 data. *Journal of Applied Meteorology and Climatology*, 47(1), 44–58. <https://doi.org/10.1175/2007jame1581.1>
- Manoli, G., Faticchi, S., Schläpfer, M., Yu, K., Crowther, T. W., Meili, N., et al. (2019). Magnitude of urban heat islands largely explained by climate and population. *Nature*, 573(7772), 55–60. <https://doi.org/10.1038/s41586-019-1512-9>
- Marelle, L., Myhre, G., Steensen, B. M., Hodnebrog, Ø., Alterskjær, K., & Sillmann, J. (2020). Urbanization in megacities increases the frequency of extreme precipitation events far more than their intensity. *Environmental Research Letters*, 15(12), 124072. <https://doi.org/10.1088/1748-9326/abcc8f>
- Nations, U. (2018). *2018 revision of world urbanization prospects*. Population Division-United Nations.
- Niyogi, D., Lei, M., Kishtawal, C., Schmid, P., & Shepherd, M. (2017). Urbanization impacts on the summer heavy rainfall climatology over the eastern United States. *Earth Interactions*, 21(5), 1–17. <https://doi.org/10.1175/ei-d-15-0045.1>
- Oke, T. R., Mills, G., Christen, A., & Voogt, J. A. (2017). *Urban climates*. Cambridge University Press.
- Pimonsree, S., Limsakul, A., Kammuang, A., Kachenchart, B., & Kamlangkla, C. (2022). Urbanization-induced changes in extreme climate indices in Thailand during 1970–2019. *Atmospheric Research*, 265, 105882. <https://doi.org/10.1016/j.atmosres.2021.105882>
- Sarangi, C., Tripathi, S., Qian, Y., Kumar, S., & Ruby Leung, L. (2018). Aerosol and urban land use effect on rainfall around cities in Indo-Gangetic basin from observations and cloud resolving model simulations. *Journal of Geophysical Research: Atmospheres*, 123(7), 3645–3667. <https://doi.org/10.1002/2017jd028004>
- Schmid, P. E., & Niyogi, D. (2013). Impact of city size on precipitation-modifying potential. *Geophysical Research Letters*, 40(19), 5263–5267. <https://doi.org/10.1002/grl.50656>
- Stine, R. (1989). An introduction to bootstrap methods: Examples and ideas. *Sociological Methods & Research*, 18(2–3), 243–291. <https://doi.org/10.1177/0049124189018002003>
- Sui, X., Yang, Z.-L., Shepherd, M., & Niyogi, D. (2024). Global scale assessment of urban precipitation anomalies. *Proceedings of the National Academy of Sciences of the United States of America*, 121(38), e2311496121. <https://doi.org/10.1073/pnas.2311496121>
- Wai, K., Wang, X., Lin, T., Wong, M. S., Zeng, S., He, N., et al. (2017). Observational evidence of a long-term increase in precipitation due to urbanization effects and its implications for sustainable urban living. *Science of the Total Environment*, 599, 647–654. <https://doi.org/10.1016/j.scitotenv.2017.05.014>
- Wieringa, J. (1986). Roughness-dependent geographical interpolation of surface wind speed averages. *Quarterly Journal of the Royal Meteorological Society*, 112(473), 867–889. <https://doi.org/10.1256/smsqj.47315>
- Xu, K., Yang, D., Yang, H., Li, Z., Qin, Y., & Shen, Y. (2015). Spatio-temporal variation of drought in China during 1961–2012: A climatic perspective. *Journal of Hydrology*, 526, 253–264. <https://doi.org/10.1016/j.jhydrol.2014.09.047>
- Yang, L., Tian, F., Smith, J. A., & Hu, H. (2014). Urban signatures in the spatial clustering of summer heavy rainfall events over the Beijing metropolitan region. *Journal of Geophysical Research: Atmospheres*, 119(3), 1203–1217. <https://doi.org/10.1002/2013jd020762>
- Yang, L., Yang, Y., Shen, Y., Yang, J., Zheng, G., Smith, J., & Niyogi, D. (2024). Urban development pattern's influence on extreme rainfall occurrences. *Nature Communications*, 15(1), 3997. <https://doi.org/10.1038/s41467-024-48533-5>
- Yang, W., Luan, Y., Liu, X., Yu, X., Miao, L., & Cui, X. (2017). A new global anthropogenic heat estimation based on high-resolution nighttime light data. *Scientific Data*, 4(1), 1–11. <https://doi.org/10.1038/sdata.2017.116>
- Zhang, S., Huang, G., Wang, J., Liu, Y., Jia, G., & Ren, G. (2015). Impact of urban surface characteristics on summer rainfall in the Beijing-Tianjin-Hebei area. *Chinese Journal of Atmospheric Sciences*, 39(5), 911–925. <https://doi.org/10.3878/j.issn.1006-9895.1411.14199>
- Zhu, X., Li, D., Zhou, W., Ni, G., Cong, Z., & Sun, T. (2017). An idealized les study of urban modification of moist convection. *Quarterly Journal of the Royal Meteorological Society*, 143(709), 3228–3243. <https://doi.org/10.1002/qj.3176>

References From the Supporting Information

- Garratt, J. R. (1994). The atmospheric boundary layer. *Earth-Science Reviews*, 37(1–2), 89–134. [https://doi.org/10.1016/0012-8252\(94\)90026-4](https://doi.org/10.1016/0012-8252(94)90026-4)